BOLTON / FARR. D

6 Energy Balance and Hydrological Processes in an Arctic Watershed

L. D. HINZMAN, D. L. KANE, C. S. BENSON, and K. R. EVERETT

6.1 Introduction

Major efforts in recent years to understand global energy and water balances have focused attention on thermal and hydrological processes in high latitudes (Kane et al. 1992). One of our objectives in the R4D program (Chap. 1, this Vol.) was to develop a quantitative understanding of hydrological processes in the Imnavait Creek watershed and the energy flows that drive them. In this chapter we present monitoring data on energy balance, evapotranspiration, precipitation, snow distribution, snowmelt, runoff, and snow damming of runoff during the spring melt. We use these data first to develop budgets and elucidate seasonal and annual patterns; subsequently, we present physical process models that further quantify the dynamics and interactions between thermal and hydrological regimes and provide additional insight with regard to water and energy budgets in tundra ecosystems.

6.2 Radiation and Thermal Regimes

The Arctic receives much less solar radiation than lower latitudes and also experiences higher annual variation, both of which affect all aspects of arctic hydrological and thermal regimes. At the Imnavait Creek watershed we measured inputs and outputs of radiation over tussock tundra, the dominant type of vegetation (see Fig. 4.7c in Chap. 4, this Vol.). These data along with air and soil temperatures have been collected between early spring (April) and late fall (October) since 1985. Data collection during the winter is more limited, due to difficulties in maintaining and servicing the station.

From October to May and before the initiation of spring snowmelt – normally a few weeks before summer solstice – the tundra surface is characterized by a homogeneous high albedo near 0.8 (Weller and Holmgren 1974). Due to the uneven distribution of snow, the surface albedo varies greatly as the melt progresses (Liston 1986). Between the period of spring snowmelt and fall snow accumulation, the tundra surface has its lowest albedo of ca. 0.2, which results in maximum energy exchange (Ohmura 1981). Short-term increases in albedo may occur during midsummer, due to snowfall, which can occur on any day of the year. Initial snow accumulation in the autumn is usually near the equinox,

J.F. Reynolds and J.D. Tenhunen (Eds.)
Ecological Studies, Vol. 120

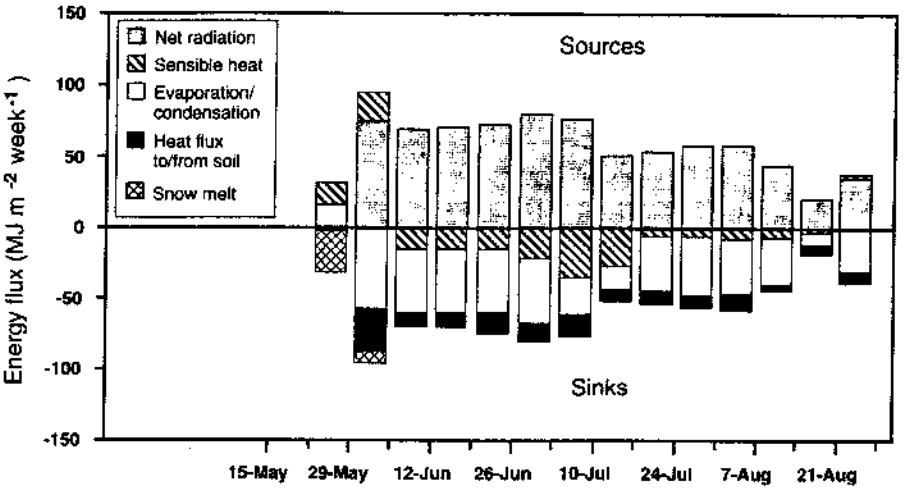

Fig. 6.1. Surface energy balance calculated in weekly increments at a point on a west-facing slope of the Imnavait Creek watershed during summer 1989

and because solar radiation is considerably less at this time, arrival of new snow cover does not produce the dramatic changes in surface energy and water fluxes that occur during spring-snow ablation (Fig. 6.1; Kane et al. 1990).

The Imnavait Creek watershed receives no direct solar radiation between 5 December and 8 January, and although several hours of diffuse radiation are incident on each day throughout the winter, the energy input is small. About 77% of the annual sunlit hours in the watershed occur between 21 March and 21 September. Incident shortwave radiation is governed by sun angle, but is greatly reduced on cloudy days. Even on clear summer days the low solar angle (maximum at summer solstice is only 45°) means that incoming solar radiation is highly attenuated by the atmosphere. The amount of shortwave radiation reflected depends on the presence of snowcover, soil moisture levels, sun angle, and radiation intensity. Atmospheric longwave radiation is primarily influenced by sky conditions and temperature. Snow ablation in spring and snow accumulation are significant factors determining the longwave radiation emitted from the surface. Net radiation becomes positive during daylight in March, increases substantially after snowmelt, as surface albedo and reflected radiation sharply decrease, and varies around a value of approximately 10 MJ m^{-2} day^{-1} (see also Kane et al. 1990) during midsummer (Fig. 6.1), as has been described at a number of other tundra sites (Barry 1981).

During the winter, arctic tundra climate is affected primarily by radiative heat loss and atmospheric circulation (Weller and Holmgren 1974; Ohmura 1981). Low incoming radiation and high albedo determine that little energy is input to the active layer (the shallow layer of soil above the permafrost that thaws – and then freezes – seasonally as a function of the net energy balance).

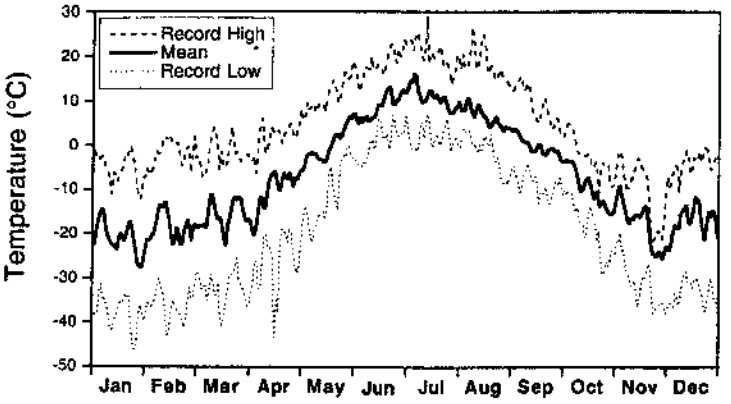

Fig. 6.2. Seven-day running mean of daily air temperature and record high and low average hourly air temperatures from January 1985 through May 1993

Mean daily air temperature and record high and low temperatures (average hourly temperatures from January 1985 to May 1993 are used in the comparison) in the Imnavait Creek watershed are presented in Fig. 6.2. The average annual air temperature during this period was −7.4 °C. Mean monthly air temperatures exhibit similar trends to data collected at Barrow (ca. 400 km NW; Dingman et al. 1980), i.e., interannual variability (expressed as standard deviation of mean monthly temperature) for the winter months is usually >3 °C, and for the summer months, usually <2 °C. This difference has been attributed to northward shifts in the arctic frontal zone during the summer (Dingman et al. 1980).

6.2.1 Surface Energy Balance

The surface energy balance is given by (terms defined in Table 6.1):

$$Q_n + Q_h + Q_c + Q_e + Q_m = 0. \quad (1)$$

Energy transferred by rain or running water was not included in this analysis, because precipitation and soil water temperature are usually close to soil temperature and, consequently, over short periods of time add little energy. This energy source may be significant when rain falls on existing snow, but this was rare during the period of our study.

Convection (Q_h), the sensible heat transferred between air and soil or snow surface, was calculated as a function of temperature gradient, wind speed, and surface conditions:

$$Q_h = C_p \cdot p_a \cdot D_h \cdot (T_a - T_{sur}), \quad (2)$$

where it is assumed that the momentum exchange coefficient between the atmosphere and ground equals the heat exchange coefficient (D_h; Szeicz et al.

Table 6.1. Definition of terms and units

Variable	Definition	Units
C	Soil heat capacity	$J m^{-3} °C^{-1}$
C_p	Specific heat of air	$J kg^{-1} °C^{-1}$
D_h	Convective transfer coefficient	$m s^{-1}$
	Neutral conditions, $Dh(n) = k^2 u_{z2}/[\ln (z_2/z_0)]^2$	
	Stable conditions, $Dh(n)/[1 + (\sigma * Ri)]$	
	Unstable conditions, $Dh(n)/[1 - (\sigma * Ri)]$	
dS	Active layer moisture storage and surface storage	mm
dT/dx	Vertical soil thermal gradient over distance x	$°C m^{-1}$
E	Evaporation	mm
e_a	Vapor pressure of the air	mb
e_{sur}	Vapor pressure of the surface	mb
F	Melt factor	$mm °C^{-1} h^{-1}$
F_t	Temperature melt factor	$mm °C^{-1} h^{-1}$
F_r	Radiation melt factor	$mm m^2 W^{-1} h^{-1}$
g	Gravitational constant	$m s^{-2}$
K	Thermal conductivity	$W m^{-1} °C^{-1}$
k	von Karman's constant	0.41
L_v	Latent heat of vaporization	
M	Snowmelt rate	$mm h^{-1}$
P	Air pressure	mb
p	Precipitation or snowmelt	mm
Q_c	Heat conduction into soil	$W m^{-2}$
Q_e	Energy utilized for evapotranspiration or condensation	$W m^{-2}$
Q_h	Convective heat transfer	$W m^{-2}$
Q_m	Energy utilized for snowmelt	$W m^{-2}$
Q_n	Net radiation	$W m^{-2}$
R	Runoff	mm
R_i	Richardson number, $[g * z_2 * (Ta - T_{sur})/[u_{z2} * (Ta + 273.15)]$	
SW_r	Reflected shortwave radiation	$W m^{-2}$
SW_s	Incident shortwave radiation	$W m^{-2}$
t	Time	s
T_a	Temperature of air at height z	°C
T_{sur}	Temperature of the surface	°C
u_{z1}	Wind speed at height 1	$m s^{-1}$
u_{z2}	Wind speed at height 2	$m s^{-1}$
z	Height of the wind speed and temperature measurement	m
z_0	Roughness length, $\exp[\{(u_{z2} * \ln(z_1)) - (u_{z1} * \ln(z_2))\}/\{u_{z2} - u_{z1}\}]$	m
ρa	Density of air	$kg m^{-3}$
σ	Constant	10
θ	Temperature	°C

1969), a relationship that holds only for neutral (isothermal) conditions. Daily heat exchange coefficients were adjusted based on the air temperature profile between the surface and 10 m using different values of D_h for neutral, stable, and unstable conditions (see Table 6.1; Braun 1985). The average surface roughness length, z_0, was determined from wind-speed profiles between 1.5 and 10 m. For tussock tundra we estimated z_o to be 0.02 m by averaging calcu-

Units
$J m^{-3} °C^{-1}$
$J kg^{-1} °C^{-1}$
$m s^{-1}$
mm
$°C m^{-1}$
mm
mb
mb
$mm °C^{-1} h^{-1}$
$mm °C^{-1} h^{-1}$
$mm m^2 W^{-1} h^{-1}$
$m s^{-2}$
$W m^{-1} °C^{-1}$
0.41
$mm h^{-1}$
mb
mm
$W m^{-2}$
$W m^{-2}$
$W m^{-2}$
$W m^{-2}$
$W m^{-2}$
mm
$W m^{-2}$
$W m^{-2}$
s
°C
°C
$m s^{-1}$
$m s^{-1}$
m
m
$kg m^{-3}$
10
°C

tions. Daily
ture profile
tral, stable,
age surface
between 1.5
ging calcu-

lations made from several hundred wind profile measurements during near-neutral conditions. This value falls well within the reported values for short grasses and tundra (Szeicz et al. 1969; Weller and Holmgren 1974). The roughness length over snow can vary a great deal as the windswept surface changes from very smooth to very rough. During the spring melt period we estimated z_0 as 0.0013 m. Effective surface temperatures were obtained from emitted terrestrial longwave radiation.

Conductive heat transfer (Q_c) is the energy passed from particle to particle within the soil matrix. Because the energy budget is calculated in a plane at the surface, it is not necessary to consider latent heat associated with the freezing or thawing of the active layer. Conductive heat transfer is calculated as:

$$Q_c = -K \cdot dT/dx. \tag{3}$$

The thermal conductivity (K) of these soils was determined for several soil types under a variety of moisture and temperature conditions (Hinzman et al. 1991b). Values of K were selected depending on whether the surface soil was wet or dry, thawed or frozen. Heat conduction into the soil was measured with heat flux plates located near the surface and at the organic-mineral soil interface. Heat flux at the soil surface largely mirrors net radiation except that diurnal variation in surface heat flux is greatly reduced during the winter because of the insulative properties of the snowpack and low variation in energy input from radiation. Daily amplitude and instantaneous magnitude of heat flux decrease with soil depth. Each spring and autumn, heat flux approaches zero as the surrounding soil progresses through a phase change. As the soil water freezes in September, energy flows from the warm soil to the colder air, and the near-surface soil temperature remains isothermal at 0 °C, because energy released as latent heat offsets surface heat loss.

Evapotranspiration can be estimated as the remainder term in a water or energy balance equation (Eq. (1)) or calculated using techniques based on vapor and wind gradients:

$$Q_e = L_v \cdot p_a \cdot D_h \cdot (0.622/P) \cdot (e_a - e_{sur}). \tag{4}$$

Because it is difficult to determine surface vapor pressure when soils are less than saturated, Eq. (4) works best during snowmelt or immediately after rainfall events. Our calculated values of Q_e compare well with values estimated from water-balance studies at Imnavait Creek (Hinzman et al. 1991a).

The importance of each of the terms in Eq. (1) varies considerably throughout the year. The rates of all energy fluxes are reduced during winter. Transpiration is zero. Conductive heat transfer is reduced by the insulating effect of the snow layer or reversed because of the temperature gradient. Evaporation is normally considered to be low during the winter because of energy constraints (Ohmura 1982). Nevertheless, the loss of snow by sublimation can be high during large wind events (Tabler 1975). Convective heat transfer is affected least by the season, but can be lower because of the

Table 6.2. Summer and annual water balances (cm)

Precipitation				Runoff			Annual evapotranspiration	
Year	Maximum snowpack water equivalent	Summer[a]	Annual total	Snowmelt	Summer[a]	Annual total	Actual	Potential[b]
1985	10.2	25.1	35.3	6.6	[c]	[c]	[c]	[c]
1986	10.9	16.3	27.2	5.7	6.2	11.9	15.3	31.0
1987	10.8	27.2	38.0	7.1	17.9	25.0	13.0	32.0
1988	7.8	25.2	33.0	3.9	7.2	11.1	21.9	33.2
1989	15.5	25.7	41.2	9.4	7.8	17.2	24.0	42.0
1990	10.6	16.3	26.9	6.4	2.8	9.2	13.3	39.4
1991	8.2	24.9	33.1	5.6	3.3	8.9	24.2	37.7
1992	18.1	24.1	42.2	14.4	6.3	20.7	21.5	32.8
1993	12.5	20.8	33.3	7.9	14.6	22.5	10.8	32.1

[a] Late June–August.
[b] Estimated from pan evaporation.
[c] No data.

smoother winter snow surface and smaller temperature gradients between snow and air.

Weekly magnitudes and variations in the various components of the surface energy budget during spring and summer 1989 are illustrated in Fig. 6.1. The spring snowpack in 1989 was the second greatest of the 9 years measured (1985–1993), but the energy balance was similar in most regards to those calculated for 1986–1992. Solar radiation is the primary source of energy during the summer months, especially after spring snowmelt. During spring melt the effect of convective heat transfer is an especially important complement to radiative heat transfer. The contribution of energy advected over the nearby Brooks Range and transferred via longwave radiation or heat convection is of primary importance in determining the initiation and rate of snowmelt. The fundamental sinks of energy are warming of the snow and soil, snowmelt, evaporation, and thawing of the active layer. In the summers of 1987, 1988, 1989, and 1990 about 39, 46, 65, and 38%, respectively, of net radiation was used in evapotranspiration (Table 6.2; Kane et al. 1990; see also Chap. 17, this Vol.). During midsummer, the surface is normally warmer than the air, due to radiative heating, and sensible heat is lost by longwave radiation and convection from the warm surface to the cooler air. Comparing the energy balance during spring melt at Imnavait watershed with other sites on the North Slope, convective heat transfer exerts more influence near the Brooks Range, and decreases in importance north onto the Coastal Plain, where net radiation plays a greater role (Weller and Holmgren 1974; Dingman et al. 1980; Hinzman et al. 1991a).

6.2.2 Snow Cover and Soil Thermal Regime

Snow distribution and snowpack volumes in the Imnavait watershed are extremely variable both in time (year to year) and space (within the watershed; Benson 1982; Liston 1986), and are largely a function of wind and topography. At the end of the accumulation season, snow depths can range from a few centimeters on windswept ridgetops to more than 1 m in the bottom of the valley. The average depth over the whole watershed is about 50 cm. This region has primarily north-flowing katabatic winds that result from downslope drainage of denser air from the Brooks Range to the south. However, large wind events can originate from any direction causing extensive drifts and wind slabs throughout the watershed. Wind slabs are characterized by very hard, fine-grained layers of snow with densities between 0.35 and 0.54 g cm^{-3}. In Imnavait watershed the direction and force of the larger wind events vary from year to year, changing the orientation of the drift sequence. Nevertheless, the consistency of the predominantly southeast wind yields similar snow distribution each year, i.e., deposition in valley bottoms and on the lee side of slopes (Fig. 6.3). The orientation of wind slabs depends on the direction of strong winds, whereas the density of the drift depends on the magnitude of the wind events.

Snow depths, measured along selected traverses, were combined with pit studies to measure snow density, temperature, and hardness profiles. In addition to providing the water equivalent of the snowpack (Fig. 6.3), pit studies allowed us to measure extreme snow types such as wind-slab and depth-hoar layers. Photographs were taken from control points on the ground at selected time intervals during each melt season. These data permitted us to extrapolate detailed point measurements over broad areas, producing maps of the maximum end-of-winter snow cover.

Whereas wind direction did not vary, year-to-year wind strengths differed significantly. In 1985 there was maximum wind slab formation and the highest snow density with maximum values of 0.54 g cm^{-3}. The sensitivity of snow distribution to topography is pronounced (Fig. 6.4). Accumulation on lee slopes was about 65% more than on windward slopes, although slope angles differed by only 2–3 degrees.

Snowpack distribution and density affect runoff processes in several ways. Because of snowdrifts, snowpack water content can vary by a factor of 2–3 over a distance of a few meters. The result is a fast melt where snowpack is thin, and the development of bare patches, with considerable edge effect around the drifts during melting. On the valley floor, where snowpack is thick and dense, it functions as a dam, holding until the force of the water overcomes the bonding strength of the snow (Kane et al. 1989, 1991a). In addition, snow accumulation near stream channels and water tracks yields a higher proportion of runoff and less evaporation than if the snow were uniformly distributed throughout the watershed. Deeper snowpacks also greatly influence the thermal regime of the underlying soil by increasing thermal resistance to heat flow.

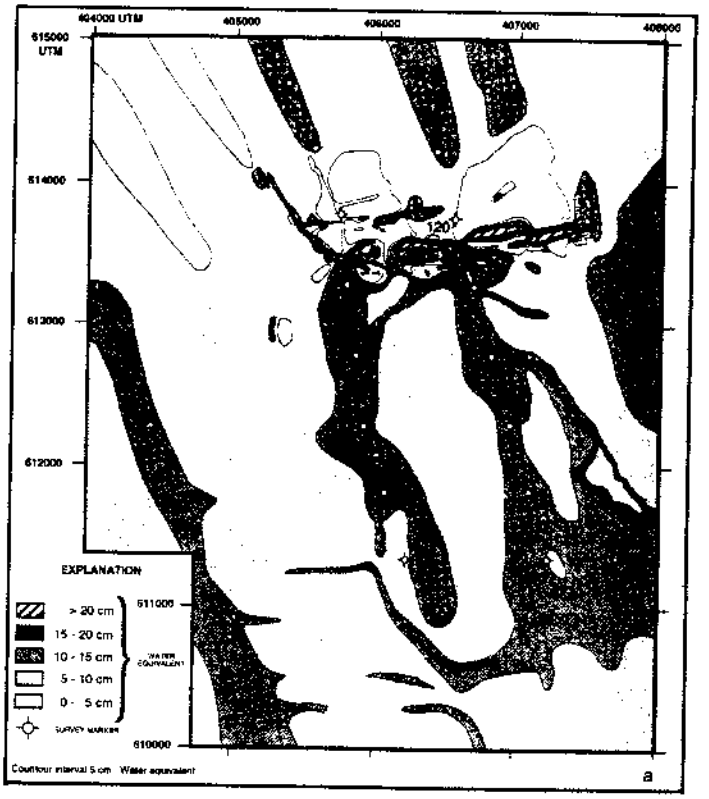

Fig. 6.3a,b. Areal snow distribution over R4D region in Spring 1988 (a one of the lowest snowpacks) and Spring 1989 (b one of the highest snowpacks). UTM grid location is illustrated in Chap. 1 (this Vol.)

Soil stratigraphy also affects the thermal regime through the insulative properties of the organic soil at the surface. The thermal conductivity of this layer is one-half to one-sixth that of the underlying mineral soil (Hinzman et al. 1991b). The albedo is also higher than mineral soil and, thus, if this surface layer is removed, heat flux increases in the exposed mineral soil.

Although air temperatures normally reach their annual minimum in January or February (Fig. 6.2), the annual minimum soil temperature normally occurs in late March or April (Fig. 6.5). Surface soil warms rapidly by 6–7°C within a few days in late May or June when solar radiation and soil heat fluxes are near annual maximum. The primary reason for the very rapid spring warming of the surficial soil layer is infiltration and freezing of snow meltwater in the still-cold soils and the release of substantial amounts of latent heat. The daily and hourly temperature variability of each layer is greatest in the summer. This variation decreases with depth. The thermal gradient reverses during autumn freeze-up and spring melt, with the soil at 40 cm warmer in winter and cooler in summer than the surface soil.

Fig. 6.3. (*continued*)

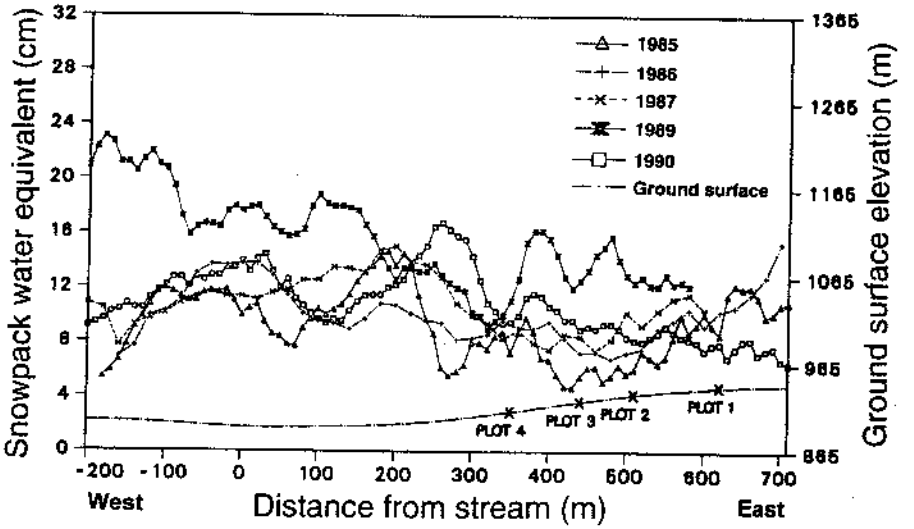

Fig. 6.4. Snowpack distribution across Imnavait Creek watershed. The four runoff plots constructed along the east slope of the watershed are depicted at their respective elevation on the ground surface line

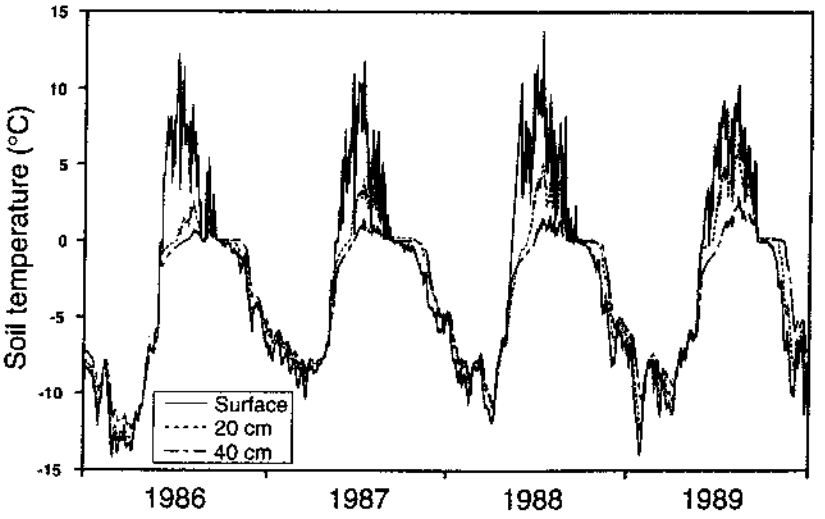

Fig. 6.5. Average daily soil temperatures measured at several depths from 1986 through 1989

In September and October, the soil begins to freeze, passing through a period of isothermal conditions. It takes longer for the active layer to freeze than to thaw in the spring, because heat transfer at the surface is less during the fall. In October, the amount of incoming radiation is much less than during the spring thaw, but the net radiation balance is still positive. The primary reason that the heat transfer rate is lower during the autumn is because of snowfall. Early-season snow will usually melt soon after touching the surface, which draws energy from the warmer soil surface to melt the snow. As the surface quickly cools to 0°C and snow begins to accumulate, heat loss slows as the snow provides insulation.

6.3 Hydrological Processes

Hydrological processes in the Arctic are similar to hydrological processes in more temperate regions (Kane et al. 1992). However, the presence of permafrost results in marked differences in the response to rainfall or snowmelt (Woo 1986). Permafrost completely underlies the Imnavait Creek watershed, affecting microclimatology, hydrological processes, and thermal regime. Ice-rich mineral soils at the permafrost table (Chap. 4, this Vol.) act as a barrier, preventing percolation from snowmelt or summer rains into deep groundwater; hence, the contribution to base flow from below the permafrost table at Imnavait Creek is zero, effectively simplifying the hydrological dynamics. Although deep springs provide water for base flow throughout the year in some places on the North Slope of Alaska (such as the adjacent

Kuparuk River system), the Imnavait Creek watershed is isolated from this subpermafrost water source. Because water is not lost to groundwater recharge, all water leaves the basin either through near-surface runoff or evapotranspiration.

The depth of the active layer ranges from 25 to 100 cm. The highly stratified soils – classified as pergelic cryaquepts or histic pergelic cryaquepts (Rieger et al. 1979; Chap. 4) – strongly influence both hydrological and thermal regimes (Hinzman et al. 1991b; Kane et al. 1992). There is a thick, porous layer of organic matter on the surface consisting of partially decomposed mosses, sedges, and other plants, which saturates and drains quickly. The underlying mineral soil is usually saturated with water. The hydraulic conductivity of the organic layer is 10–1000 times greater than that of mineral soil (Hinzman et al. 1991b). Consequently, water from snowmelt or summer rainfall moves rapidly downslope above the organic–mineral interface. An analysis of streamflow hydrographs reveals that as summer progresses, the recession curves of stream discharge following a rain event increase slightly. This observation indicates that the percentage of hillslope runoff flowing through the mineral soils increases slightly as the active layer increases in thickness, although most of the runoff still flows through the organic mat (Hinzman et al. 1993).

6.3.1 Snowmelt

The start of spring snowmelt in the Imnavait Creek watershed varies greatly depending on the depth of snowpack and meteorological conditions. From 1985 to 1993 the date of initial melt ranged from 8 May to 1 June with an average of only 10 days required for complete ablation (Fig. 6.6). An analysis of snowmelt onset as a function of initial snowpack water equivalent showed that 67% of the variation in the initiation of snowmelt could be explained by the amount of snow (dashed line in Fig. 6.6). During snowmelt, net radiation along with convective heat transfer dominate the surface energy balance (Fig. 6.1; Hinzman et al. 1991a). Although incoming shortwave radiation is very high, no melt will usually occur until convective heat transfer becomes positive.

Within a few days of a sustained melt the entire watershed becomes a patchwork of snow-covered and bare tundra. Liston (1986) found temperatures averaging 15 °C in 1985 and 24 °C in 1986 with an extreme temperature of 42 °C on bare tundra surfaces surrounded by snow, while the bordering snow was isothermal at 0 °C. Complex patterns of stable and unstable air result from strong thermal gradients. Longwave radiation emitted from snow-free ground warms the overlying air, and turbulent transfer in these locations accelerates melting of the surrounding snow. The west-facing slope melts off sooner than the rest of the watershed, because it retains less snow (see Figs. 6.3 and 6.4). The west-facing slope also receives more direct solar radiation in the afternoon when air temperatures are highest. The result is a complementary summation of radiant and convective heat transfer that results in a greater positive surface

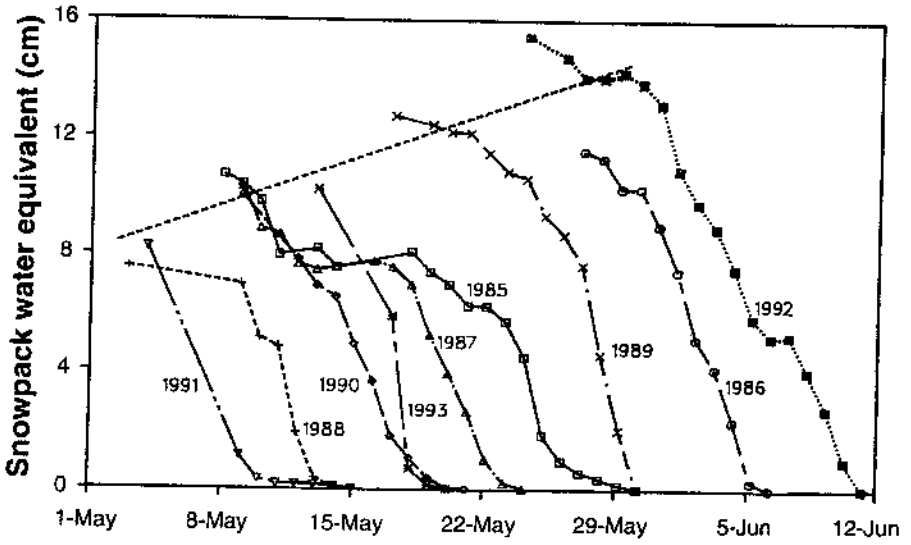

Fig. 6.6. Rates of snowpack ablation characterized by amount of snow still present as a function of time. Regression of dependence of snowmelt initiation (y) on initial snowpack water equivalent (x) is $y = 0.225\ x + 7.80$, $r^2 = 0.67$. Date of initial melt determined by the first date to show decrease in snowpack water equivalent

heat flux. The east-facing slope, in contrast, receives its maximum irradiance in the morning while convective heat transfer is smaller.

Problems in modeling snowmelt for the Imnavait watershed from surface energy balance relate to the large spatial variability in snow depth, which affects albedo, longwave emittance, and sensible heat flux. The energy balance presented in Fig. 6.1 was calculated based on instrumentation located at a single point on the west-facing slope. The measured and calculated snowpack ablation (Fig. 6.6) also represents processes occurring only on the west-facing slope (78% of the basin). A comprehensive formulation of watershed snowmelt runoff would require measurement of the surface energy balance at many points throughout the watershed. Figure 6.1 probably overestimates the magnitude of net radiation on the east-facing slope. The difficulty in calculating heat transfer and a surface energy balance in such situations has stimulated the development of a number of simplified methods for estimating rates of snowmelt (Bergström 1986; Sand 1990).

6.3.2 Plot and Basin Water Balance

Rainfall each autumn ensures that the active layer will be saturated at the beginning of each winter. Because the moisture stored in the soil is nearly the same at the end of each thaw season, it is straightforward to estimate annual water balances. Four 89-m^2 plots were constructed along a diagonal on the

ent as a function
ck water equiva-
rst date to show

m irradiance

from surface
depth, which
ergy balance
located at a
ed snowpack
e west-facing
ed snowmelt
nce at many
tes the mag-
n calculating
imulated the
ing rates of

rated at the
is nearly the
mate annual
onal on the

west-facing slope in tussock tundra to directly measure surface runoff and subsurface water flow above the permafrost (see Fig. 9.2 in Chap. 9 for location of plots). Each plot was bounded with heavy plastic, which isolated the area from upslope water. A gutter system at the base of each plot routed the water into a holding tank instrumented with a water-level recorder that provided data on runoff rates and volumes. Although these plots provided valuable information on the components of the water balance at these sites (Hinzman et al. 1993), they cannot be considered replicates, due to the large spatial heterogeneity within the watershed. The proportion of a snowpack or soil moisture that is lost either to runoff or evaporation is affected by slope and aspect; consequently, these plots may not reflect the magnitude of processes occurring elsewhere in the watershed.

The snowpack water equivalent of each plot and the basin average were determined before snowmelt began and daily during spring melt. Runoff was measured directly. The proportion of moisture going into storage in the desiccated organic layer during snowmelt was estimated in laboratory and field studies to average 1.5 cm over the entire basin (Kane et al. 1989). Evaporation was calculated as:

$$E = p - R - dS. \tag{5}$$

During this study the initial snowpack on each plot ranged between 7.2 and 14.7 cm, and basin averages ranged between 7.8 and 18.1 cm. Evaporation varied greatly depending on the initial water content of the snowpack, proportionally increasing as the snowpack decreased. On the basin scale the amount of runoff depended primarily on the amount of snow, but distribution of the snow was important in determining the fraction going into runoff or evaporation (Table 6.2). When more snow was deposited in the bottom of the watershed, near the stream, runoff was greater and evaporation was lower. The processes associated with spring melt and runoff are discussed in more detail in Kane and Hinzman (1988) and Kane et al. (1989, 1991a).

6.3.3 Runoff and Basin Discharge

Frequently, there were large differences in the depth of snowpack along the hillsides (Figs. 6.3 and 6.4), which strongly affected basin runoff. Compared with plots having an average snowpack water equivalent, runoff on plots with a thin snowpack began earlier, probably because of a lower albedo, greater shortwave absorbance by the underlying soil, and greater longwave emittance from shrubs protruding through the snow surface. Plots with thinner snowpacks also lost a greater proportion of water to evaporation. Plots with the deepest snowpacks had the greatest runoff volumes and the greatest peak flows.

During spring melt most downslope water movement occurs in the top 10 cm of the organic layer (Hinzman et al. 1991b). Moisture content at 5 cm

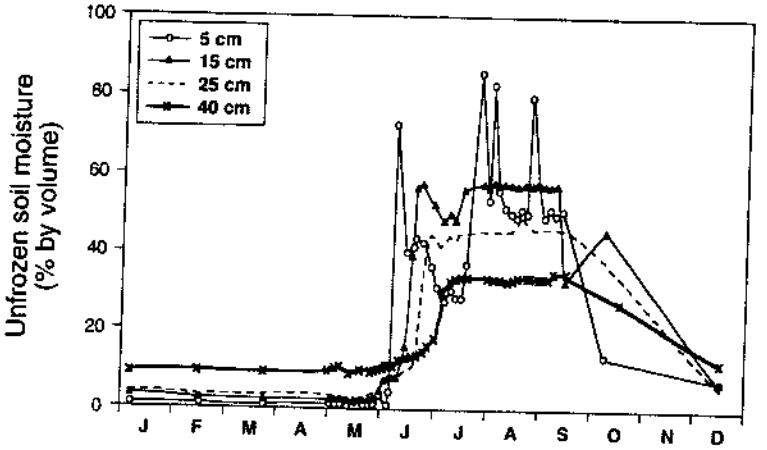

Fig. 6.7. Unfrozen soil moisture content during 1986 measured at several depths with time-domain reflectometry (Hinzman et al. 1991b)

increases abruptly as meltwater begins to infiltrate (Fig. 6.7), but the moisture content below this layer did not substantially increase until snowmelt was complete and the depth of thaw reached below 10 cm. As the surficial organic layer becomes saturated, an intricate flow occurs in discontinuous rills between sedge tussocks. Over time the ice-rich soil thaws, releasing water and maintaining the mineral soil near saturation throughout the year. However, the moisture content of the organic soil varies greatly throughout the year. The moisture content of surface organic soils varies by as much as 60% by volume throughout the summer (Fig. 6.7), saturating and drying quickly in response to summer rains or snowmelt. Subsurface mineral soils, in contrast, remain near saturation (Hinzman et al. 1991b).

Flow alternates between the surface and subsurface depending on soil conditions, topography, and depth of thaw. The highly porous moss layer and well-developed intertussock channels are conducive to rapid downslope movement. The hillside is drained by small water tracks that are nearly parallel to each other (ca. 50 m apart; see Fig. 4.4 in Chap. 4, this Vol.). Following a precipitation event, these water tracks fill with water and quickly drain the hillslope (Kane et al. 1991a). As the melt season progresses and the depth of thaw increases, the amount of moisture storage increases. Thus, runoff and soil moisture dynamics are a function of seasonal time, an attribute that has significant implications for modeling the hydrological regime especially considering the effects of disturbance (Hinzman and Kane 1991).

The drainage is a beaded ephemeral stream that flows from spring melt until freeze-up in September. Spring runoff is usually the dominant hydrological event of the year (Kane and Hinzman 1988), producing the annual peak flow and about 50% of the total annual runoff volume. Streamflow almost ceases after extended periods of low precipitation, which may occur in late

Table 6.3. Average daily evapotranspiration calculated from an hourly energy balance in the Imnavait Creek watershed (mm day^{-1})

	1987	1988	1989	1990	Average
May	0.6	1.0	0.5	1.7	1.0
June	2.7	1.5	3.0	1.1	2.1
July	0.8	2.0	2.0	0.8	1.4
August	0.6	2.1	1.9	1.5	1.5

May or June, whereas intense summer rainfall events produces substantial stream flow (see also Chaps. 9 and 17, this Vol.).

6.3.4 Precipitation, Evaporation, and Evapotranspiration

Based on the 8-year record from 1985 until 1992, the average annual precipitation is ca. 35 cm, two-thirds of which falls in late June, July, and August (Table 6.2). The period in the Arctic with the least sea ice falls in late July and August (Labelle et al. 1983) corresponding to the period of greatest precipitation. The total number of rain events recorded for the summers of 1985–1988 was 256. A substantial number of these reflect discontinuous periods of precipitation (many of them too light to be recorded by a standard rain gauge) within protracted periods of rainy weather. Most rainfall is light (95% at rates <10 mm h^{-1} and 82% < 1.0 mm h^{-1}), appears evenly distributed over the catchment, and is associated with the dissipating phase of convective storms generated over the Brooks Range or with air masses moving from the North Pacific Ocean. Maximum rainfall intensities generally occur in the first 4 or 5 hours of the event. High-intensity (>20 mm h^{-1}), short-duration rainfall is associated with convective storms which generally occur earlier in summer.

Actual and potential evapotranspiration (Table 6.2) and average daily evapotranspiration per month (Table 6.3) indicate that both evapotranspiration and pan evaporation are generally greatest after snowmelt and decrease throughout the summer. On hillslopes with good drainage the rate of evaporation is possibly limited by the degree of hydration of mosses. In marshy areas of the valley bottom, the free water surface frequently lies above the soil surface so that the rate of evaporation is limited by the amount of available energy. Rates of evapotranspiration were calculated according to the energy balance (Sect. 6.2.1) and with the Priestley-Taylor method (Priestley and Taylor 1972; Kane et al. 1990). The predictions for summer 1987 are compared with precipitation and pan evaporation in Fig. 6.8. During the early summer, evapotranspiration rates are greater than precipitation indicating watershed drying. This drying of the active layer occurred regularly following spring snowmelt and significantly modifies decomposition (Chap. 16), nutrient availability (Chap. 10), and carbon balance (Chaps. 11 and 17).

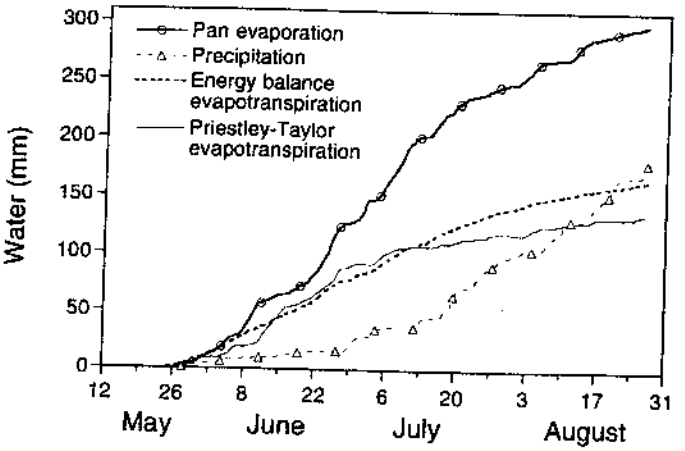

Fig. 6.8. Comparison of cumulative precipitation, pan evaporation and calculations of evapotranspiration during the summer of 1987. (from Kane et al. 1990)

6.4 Energy Balance and Hydrology Models

6.4.1 Simulation of the Thermal Regime

The thermal regime of the top 60 m of soil in tussock-tundra plots was simulated using the Two-Dimensional Heat Conduction (TDHC) model, a finite element computer simulator that allows non-steady-state analysis (Goering and Zarling 1985). This is a physical model based on heat conduction and phase change. The TDHC model utilizes the following formulation of the heat-diffusion equation.

$$\frac{\partial}{\partial x}\left[K\frac{\partial\theta}{\partial x}\right]+\frac{\partial}{\partial y}\left[K\frac{\partial\theta}{\partial y}\right]=C\frac{\partial\theta}{\partial t}, \tag{6}$$

where x and y are the coordinates (m) in the horizontal and vertical directions, respectively, θ is temperature, K is the thermal conductivity, C is heat capacity, and t is time (see Table 6.1). A two-dimensional grid of linear triangular elements of variable size was created vertically in the soil profile where the top of the grid corresponded to the soil surface. The elements were smallest near the surface where soil thermal properties and soil temperatures changed quickly and increased in size with depth. The grid contained 255 nodes and 336 elements; the simulation time step was 1 day. The lower boundary of the grid was selected as 61 m to ensure only negligible change in the temperature of the lower boundary in response to surface perturbations.

Equation (6) is solved using a finite element technique based on the Galerkin weighted-residual process. The simulations are driven by the surface temperature and heat flux at the bottom of the grid. Information must also be

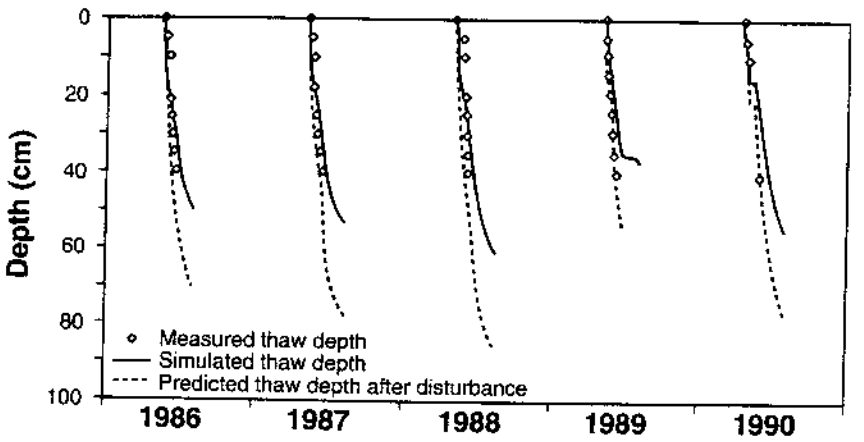

Fig. 6.9. Comparison of simulated thaw depths with and without surface disturbance (removal of organic soil layer)

provided on the frozen and thawed thermal conductivity, frozen and thawed heat capacity, and the amount of latent heat required for phase change in each soil element. The amount of heat transferred during phase change in each element is calculated using a Dirac delta function (O'Neill 1983). Heat flux at the lower boundary was estimated at 0.050 W m^{-2} based on an analysis of soil thermal properties and the geothermal gradient of a deep well 15 km from the Imnavait watershed (Osterkamp et al. 1987). The model accuracy was verified by testing it against closed form exact solutions (Goering and Zarling 1985; Zarling et al. 1989).

The model was calibrated and used to simulate rates of thaw of the active layer in the Imnavait Creek watershed during the years 1985–1990 (Fig. 6.9; Kane et al. 1991b). Simulated temperatures at several soil depths were compared with continuous measurements of actual subsurface temperatures. In the active layer, predicted temperatures were within 0.25 °C of observed temperatures 75% of the time, within 0.50 °C of observed temperatures 92% of the time, and within 1 °C of observed temperatures 96% of the time. Thus, reasonable agreement was also obtained between observed and simulated thaw in the active layer (Fig. 6.9). The TDHC model simulated the observed temperature gradients extremely well during periods when the soil was completely frozen and heat flow was entirely via conduction.

To examine sensitivity of the thaw processes to surface modification as described by TDHC, we simulated an extreme case of disturbance in which the surficial organic layer is stripped off (Fig. 6.9), a situation that occurred during the early years of development in Alaska (Chap. 4, this Vol.; Parker 1929). Due to the greater heat conductivity of the mineral soil, thaw proceeds rapidly and reaches greater depth by the end of the season (ca. 20–30 cm). The subsurface temperatures near the surface of the disturbed soil profile are colder in the coldest part of winter and warmer in the warmest part of summer, in effect

Table 6.4. Soil temperatures at three depths during 1987 simulated using two-dimensional heat conduction (TDHC) in cases where the soil was undisturbed and when the surficial organic layer was removed (disturbed)

	10 cm		20 cm		30 cm	
	Undisturbed	Disturbed	Undisturbed	Disturbed	Undisturbed	Disturbed
Jan	−6.63	−6.62	−6.24	−6.21	−5.30	−5.17
Feb	−7.79	−7.82	−7.52	−7.55	−6.42	−6.37
Mar	−8.46	−8.52	−8.41	−8.45	−7.47	−7.45
Apr	−7.88	−7.89	−7.77	−7.78	−7.25	−7.23
May	−0.31	−0.20	−1.50	−1.38	−4.11	−4.04
June	1.00	3.15	−0.10	1.76	−1.78	−1.48
July	2.67	4.06	1.00	2.74	−0.95	−0.63
Aug	1.89	2.84	0.97	2.13	−0.62	−0.25
Sept	−0.02	0.01	0.02	0.01	−0.49	−0.19
Oct	−0.22	−0.19	0.00	0.03	−0.45	−0.18
Nov	−2.11	−2.01	−0.99	−0.61	−0.45	−0.19
Dec	−5.61	−5.07	−5.06	−3.52	−3.59	−0.11

changing the amplitude and the lag time of the annual temperature cycle (Table 6.4). Although thaw depth changes are small, such changes can lead to the melting of ground ice, the formation of depressions in which surficial runoff and infiltration water may accumulate, and thermal erosion. On hillsides, the fine-grained mineral soils offer little resistance to the erosion process (Mageau and Rooney 1984).

6.4.2 Simulation of Snowmelt

The physically correct method to quantify snowmelt is by determining a complete energy balance for the snowpack (Sand 1990). However, the processes of heat transfer within and to the snowpack are highly variable, both spatially and temporally, and are extremely difficult to define (Male and Granger 1981). The complexity of this approach has led to development of many simplified snowmelt equations (Bengtsson 1976; Bengtsson 1982).

We computed rates of snowmelt within the Imnavait Creek catchment using three different approaches (Fig. 6.10): an energy balance model (Price and Dunne 1976), a "degree day method", and a modified "degree day method" that includes radiation influences. The second approach used the following empirical equation:

$$M = \begin{cases} F\,(T_a - T_o) & \text{when } T_a > T_o \\ 0 & \text{when } T_a \le T_o, \end{cases} \qquad (7)$$

Where M is the snowmelt rate, F is the melt factor, and T_a and T_o are air and threshold temperatures, respectively (Table 6.1). When $T_a < T_o$, melt will not

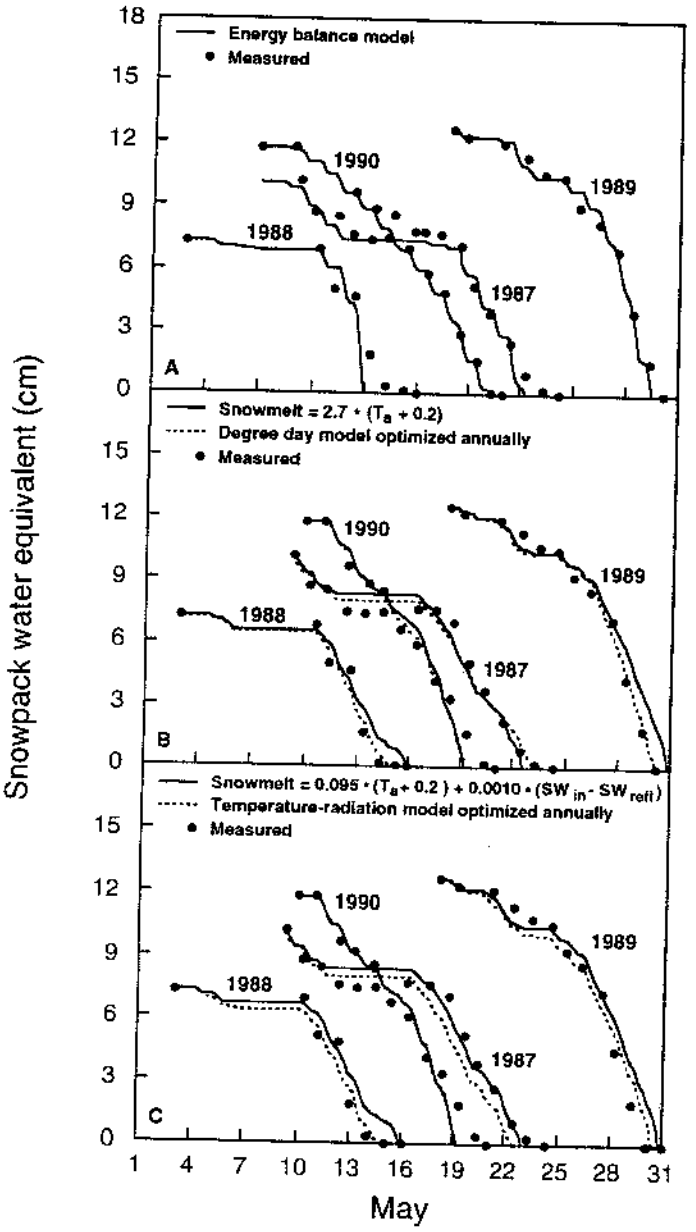

Fig. 6.10A–C. Simulated and observed snowpack ablation in Imnavait Creek watershed during spring melt 1987–1990 using A an energy balance model; B a degree-day model [Eq. (7)]; and C a temperature/radiation index model [Eq. (8)]

occur. The threshold is normally less than 0°C, due to the effect of solar radiation. It is necessary to know when the snowpack is isothermal at 0°C before the calculations can be initiated. The inclusion of a simple solar radiation term in Eq. (7) slightly improves performance, i.e.:

$$M = F_t (T_a - T_o) + F_r (SW_s - SW_r), \quad (8)$$

Where F_t is the temperature melt factor, F_r is the radiation melt factor, and SW_s and SW_r are incident and reflected shortwave radiation, respectively (Table 6.1). As seen in Fig. 6.10, the energy balance approach provided the best results; however, the simple approaches also performed well. The empirical methods deviated from observation as the snowpack water equivalent decreased. Comparison of panels B and C in Fig. 6.10 suggests that snowmelt within the Imnavait Creek watershed is largely controlled by the sensible heat component of the energy balance (Hinzman et al. 1991a), whereas radiation is of lesser importance. Radiation does play a much greater role in the process of snowmelt on the Arctic Coastal Plain (Weller and Holmgren 1974; Hinzman et al. 1991a).

6.4.3 Simulation of Catchment Runoff

Water balance was examined with the hydrological model, HBV (HBV refers to Swedish Meteorologic and Hydrologic Institute's model; Bergström 1976), for the summer season during the years 1986–1989. Of 40 important parameters in HBV, 26 describe the basin and the input data, whereas the remainder collectively describe snow accumulation and ablation, soil moisture accounting, and generation or transformation of runoff (Hinzman and Kane 1991). A number of parameters are empirically determined via calibration procedures for the watershed. Data collected during the summer of 1986 provided the primary calibration. Snowmelt is calculated with a degree-day formulation (Hinzman et al. 1991a). This simplification seems acceptable, because the parameters of the model were optimized to best simulate discharge and not ablation (Hinzman and Kane 1991). As the thickness of the active layer increases, field storage capacity increases. The mechanisms of runoff are controlled primarily by the properties of the near-surface organic soils (Hinzman et al. 1991b, 1993).

The HBV predicts stream flow well and also provides reasonable estimates of daily evapotranspiration and soil moisture levels. The HBV performs best in reconstructing simple discharge events such as the snowmelt or rainfall events of 1986 (see hydrograph in Chap. 17, this Vol.). The three major summer precipitation events were very distinct and not complicated by overlapping recession curves. The first two events after the spring melt were caused by rainfall, and the third event was a summer snowmelt event. The HBV considers the state of summer precipitation, i.e. snow or rain, and determines runoff appropriately. It proved difficult to adequately describe many of the 1987

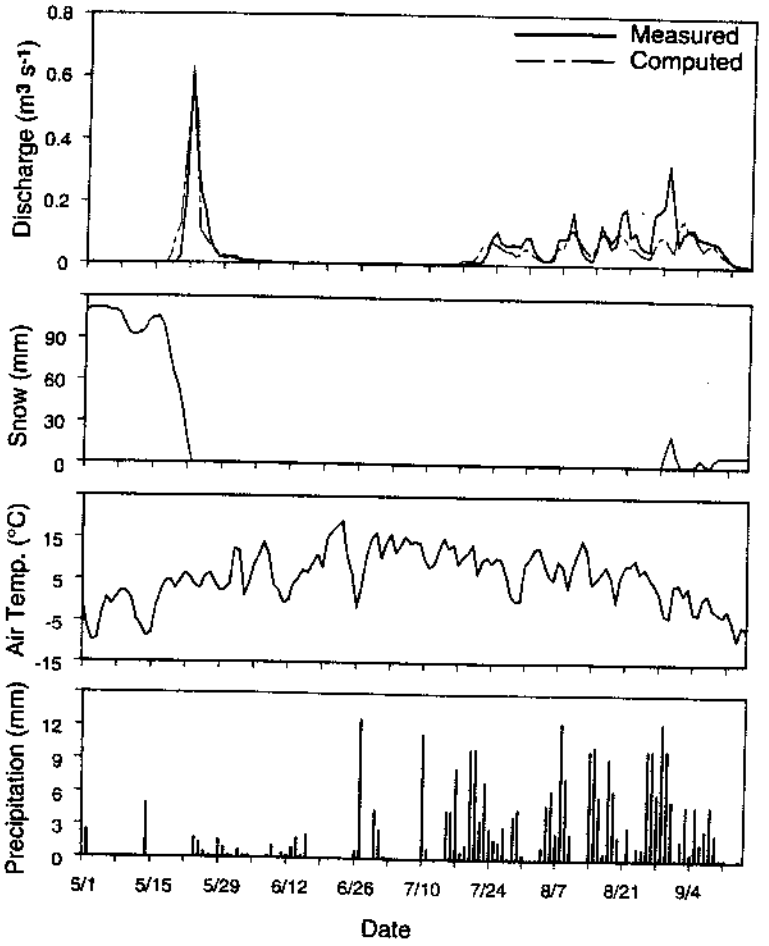

Fig. 6.11. Stream flow observed and simulated by HBV model, predicted snowpack ablation, measured air temperature and precipitation in 1987

summer events (Fig. 6.11), because precipitation fell as mixed snow and rain, and a series of storms resulted in overlapping recession curves.

An important objective in this analysis was to identify basin characteristics that appeared to be sensitively related to runoff discharge as described by model parameters. To predict discharge four key parameters were varied during the summer: (1) the threshold temperature for onset of snowmelt; (2) maximum soil moisture storage in the model; (3) maximum soil moisture storage in the upper reservoir; and (4) a parameter in the soil moisture routine that is influenced by the thickness of the active layer (Hinzman and Kane 1992). The threshold temperature must change after spring melt, because energy from the surficial soils contribute to the melting of summer snow. The

simulations were sensitive to changing catchment water-storage capacitance that results from the progression of soil thawing.

6.5 Conclusions

Spring melt is the dominant hydrological event of the year in the Imnavait Creek watershed, usually lasting only about 10 days, but normally releasing about half the annual surface runoff and producing the annual peak flow. Net radiation is low or negative throughout the winter, increasing abruptly after snowpack ablation. Convective heat transfer is important during snowmelt, and when it complements radiation, snowmelt may occur rapidly. The volume and distribution of the snowpack within the watershed has a substantial impact on the timing, rates, and mechanisms of snowmelt and subsequent runoff. Total yearly precipitation averages ca. 35 cm, about one-third to one-half occurring as snowfall. Because no surficial water may percolate through the permafrost into subpermafrost groundwater, evaporation and runoff are the major pathways of water loss from the watershed. Surficial runoff occurs primarily within the highly porous near-surface organic soils, although as the active layer thaws through the summer, the small proportion of water flowing through the mineral soil increases slightly. During the summer, the total water loss through evapotranspiration may match or exceed the total leaving the watershed as runoff.

The thermal model, TDHC, was a very good predictor of the thermal regime of the active layer, both spatially and temporally. The model showed that conduction is the major mechanism of heat transfer in environments dominated by frozen soils, although phase change is a significant process. The TDHC model was used to estimate the depth of thaw and temperature profiles in soils following surface disturbance. As expected the disturbed soils experience greater thaw depths and greater year-to-year variability. The hydrological model, HBV, satisfactorily described the significant hydrological processes of this arctic watershed including evapotranspiration, infiltration, soil moisture fluctuations, runoff, snowmelt, and snow damming. In this model, a simple temperature-index method was used to predict snowmelt.

Acknowledgments. This research was sponsored by the US Department of Energy, Office of Health and Environmental Research, Ecological Research Division. Elizabeth K. Lilly and Robert E. Gieck assisted in every aspect of this research.

References

Barry RG (1981) Tundra climates. In: Bliss LC, Heal OW, Moore JJ (eds) Tundra ecosystems: a comparative analysis. Cambridge Univ Press, Cambridge, pp 241–256

Bengtsson L (1976) Snowmelt estimated from energy budget studies. Nordic Hydrol 7: 3–18

Bengtsson L (1982) The importance of refreezing on the diurnal snowmelt cycle with application to a northern Swedish catchment. Nordic Hydrol 13: 1–12

Benson, CS (1982) Reassessment of winter precipitation on Alaska's arctic slope and measurements on the flux of wind-blown snow. Research Report UAG R-288. Geophysical Institute, University of Alaska, Fairbanks. 26p

Bergström S (1976) Development and application of a conceptual runoff model for Scandinavian catchments. Swed Meteorol Hydrol Inst, Norrköping, Sweden, Rep RHO7

Bergström S (1986) Recent developments in snowmelt-runoff simulation. In: Kane D (ed) Proc Symp: Cold regions hydrology. Am Water Resources Assoc, Fairbanks, Alaska, pp 461–468

Braun LN (1985) Simulation of snowmelt-runoff in lowland and lower alpine regions of Switzerland. Züricher Geogr Schr 21, Geogr Inst, Eidgenössische Technische Hochschule, Zürich, Switzerland

Dingman SL, Barry RG, Weller G, Benson C, LeDrew EF, Goodwin CW (1980) Climate, snowcover, microclimate and hydrology. In: Brown J, Miller PC, Tieszen LL, Bunnell FL (eds) An arctic ecosystem. The Coastal Tundra at Barrow, Alaska. Dowden, Hutchinson and Ross, Stroudsburg

Goering DJ, Zarling JP (1985) Geotechnical thermal analysis with a microcomputer. Civil Engineering in the Arctic Offshore. Am Soc Civil Engineers, New York, pp 604-616

Hastings SJ, Luchessa SA, Oechel WC, Tenhunen JD (1989) Standing biomass and production in water drainages of the foothills of the Philip Smith Mountains, Alaska. Hol Ecol 12: 304–311

Hinzman LD, Kane DL (1991) Snow hydrology of a headwater arctic basin 2. Conceptual analysis and computer modeling. Water Resour Res 27: 1111-1121

Hinzman LD, Kane DL (1992) Potential response of an arctic watershed during a period of global warming. J Geophys Res – Atmospheres 97: 2811–2820

Hinzman LD, Kane DL, Gieck RE (1991a) Regional snow ablation in the Alaskan Arctic. In: Prowse T, Ommanney C (eds) Northern hydrology: selected perspectives. NHRI Symp 6, Natl Hydrol Res Inst, Saskatoon, Saskatchewan, pp 121–140

Hinzman LD, Kane DL, Gieck RE, Everett KR (1991b) Hydrologic and thermal properties of the active layer in the Alaskan Arctic. Cold Reg Sci Technol 19: 95–110

Hinzman LD, Kane DL, Everett KR (1993) Hillslope hydrology in an arctic setting. Proc Permafrost 6th Conf. Beijing, China, South China Univ Technol Press, pp 267–271

Kane DL, Hinzman LD (1988) Permafrost hydrology of a small arctic watershed. In: Senneset K (ed) Proc 5th Int Conf Permafrost, Tapir, Trondheim, Norway, pp 590–595

Kane DL, Hinzman LD, Benson CS, Everett KR (1989) Hydrology of Imnavait Creek, an arctic watershed. Holarct Ecol 12: 262–269

Kane DL, Gieck RE, Hinzman LD (1990) Evapotranspiration from a small Alaskan arctic watershed. Nordic Hydrology 21: 253–272

Kane DL, Hinzman LD, Benson CS, Liston GE (1991a) Snow hydrology of a headwater arctic basin. 1. Physical measurements and process studies. Water Resour Res 27: 1099–1109

Kane DL, Hinzman LD, Zarling JP (1991b) Thermal response of the active layer in a permafrost environment to climatic warming. Cold Reg Sci Technol 19: 111–122

Kane DL, Hinzman LD, Woo M, Everett KR (1992) Arctic hydrology and climate change. In: Chapin FS III, Jefferies RL, Reynolds JF, Shaver GR, Svoboda J (eds) Arctic ecosystems in a changing climate. Academic Press, New York, pp 35–57

Labelle JC, Wise JL, Voelker RP, Schulze RH, Wohl GM (1983) Alaska marine ice atlas. Arctic Environ Inf Data Center, Univ Alaska, Anchorage

Liston GE (1986) Seasonal snowcover of the foothills region of Alaska's arctic slope: a survey of properties and processes. MS Thesis, Univ Alaska, Fairbanks

Mageau DW, Rooney JW (1984) Thermal erosion of cut slopes in ice-rich soil. State of Alaska, Dept Trans Public Facilities, Rep FHWA-AK-RD-85-02
Male DH, Granger RJ (1981) Snow surface energy exchange. Water Resour Res 17: 609–627
Ohmura A (1981) Climate and energy balance on arctic tundra, Canadian Arctic Archipelago, spring and summer 1969, 1970 and 1972. Geogr Ins, Eidgenössische Technische Hochschule Zürich, Heft 3
Ohmura A (1982) Evaporation from the surface of the arctic tundra on Axel Heiberg Island. Water Resour Res 18: 291–300
O'Neill K (1983) Fixed mesh finite element solution for cartesian two dimensional phase change. J Energy Resour Technol 105: 436–441
Osterkamp TE, Gosink JP, Kawasaki K (1987) Measurements of permafrost temperatures to evaluate the consequences of recent climate warming. State of Alaska, Dept Trans Public Facilities, Rep AK-RD-88-05
Parker GA (1929) The evolution of placer mining methods in Alaska. BS Thesis, Alaska Agric College, Fairbanks
Price AG, Dunne T (1976) Energy balance computations of snowmelt in a subarctic area. Water Resour Res 12: 686–694
Priestley CHB, Taylor RJ (1972) On the assessment of surface heat flux and evaporation using large-scale parameters. Monthly Weather Rev 100: 81–92
Rieger S, Schoephorster DB, Furbush CE (1979) Exploratory soil survey of Alaska. USDA Soil Conserv Serv, Washington DC
Sand K (1990) Modeling snowmelt runoff processes in temperate and arctic environments. PhD Thesis, Norwegian Inst Technol, Univ Trondheim
Szeicz G, Endrdi G, Tajchman S (1969) Aerodynamic and surface factors in evaporation. Water Resour Res 5: 380–394
Tabler RD (1975) Estimating the transport and evaporation of blowing snow. In: Snow Management on the Great Plains Symposium. Univ Nebraska Agric Exp Station, Lincoln, Nebraska Great Plains Agric Council Publ 73, pp 85–104
Weller G, Holmgren B (1974) The microclimates of the arctic tundra. J Appl Meteorol 13: 854–862
Woo MK (1986) Permafrost hydrology in North America. Atmos-Ocean 24: 201–234
Zarling JP, Braley WA, Pelz C (1989) The modified Berggren method: a review. Proc 5th Int Conf Cold Regions Engineering, Am Soc Civil Engineers, New York, pp 263–273